Publishing Excellence Inspiring Progress
ARISTON PUBLICATIONS
Science of Alloys and Glasses
ISSN: 3143-0732 https://aristonpubs.com/journal/science-of-alloys-and-glasses https://doi.org/10.69626/sag.2025.0191

RESEARCH ARTICLE

Recycling Assessment and Ethical Considerations of Parkia Pods Ash (PPA) Composites as a Non–Toxic Alternative for Sustainable Gamma Radiation Shielding Applications

Usman Sani [1, 2,*], U. Ibrahim [2], A. A. Mundi [2], M. M. Idris [2], Rabiatu Mahadi [1], U. M. Kankara [3]

ABSTRACT: This study aims at assessing the recycling and ethical considerations of Parkia Pods Ash (PPA) composites as a non-toxic alternative for sustainable gamma radiation shielding applications. The sample was heated and converted to ash at 400 °C for 2 hours using a muffle furnace. The sample was characterized using EDXRF, XRD, and TGA/DTA analyses, and the attenuation parameters were simulated using PHY-X software. The EDXRF confirmed the total elements present in the sample, which include Bi, W, K, Si, Fe, Ca, Sn, P, and Cl, while the XRD analysis confirmed the crystalline structure of the sample ranging from 29-55° at 2θ. The sample demonstrates slow decomposition starting at 295 °C. The sample dehydrated at 520 °C and carbonized at 900 °C with a residue of 19%, confirming the high temperature resistance and thermal stability of the PPA. The PHY-X simulation results showed a significant improvement in the shielding profile of the ash sample. The Mass Attenuation Coefficient (MAC) and Linear Attenuation Coefficient (LAC) significantly decreased from 0.128 to 0.028 cm^2/g and 0.090 to 0.020 cm^{-1} at energy levels of 0.284 MeV to 15.00 MeV, for MAC and LAC, respectively. This indicates transitions in the gamma interaction region from photoelectric effect to Compton scattering. In addition, low-energy attenuation was recorded to be high, as indicated by the decrease in HVL from 35.26 cm to 7.71 cm, TVL from 117.15 cm to 25.61 cm, and MFP from 50.88 cm to 11.12 cm. The sample demonstrated a high Z efficiency of 20.49 at the photoelectric effect region and 19.71 at the Compton scattering region. The effective atomic number (Z_{eff}) ranged approximately from 23 to 48. A low transmission factor of 0.90 at 0.284 MeV and 1.00 cm thickness was recorded. Additionally, the sample demonstrated superior radiation protection efficiency. The findings signify that the PPA sample demonstrates high shielding capability in terms of crystallinity, high temperature resistance, thermal stability, and efficient MAC, LAC, and Z_{eff}, as well as low attenuation. Therefore, PPA can be utilized as a non-toxic alternative and an excellent additive to be incorporated in glasses, concretes, alloys, and tungsten for effective gamma shielding applications.

Keywords: Parkia Pods Ash (PPA), Gamma Radiation Shielding, Attenuation Parameters, Non-Toxic Additives, Sustainable Materials, Waste-to-Wealth Recycling

Received: 12 June 2025; Revised: 14 August 2025; Accepted: 11 September 2025; Published Online: 03 October 2025

[1] Department of Physics Umaru Musa Yar'adua University, Katsina-Nigeria.
[2] Department of Physics Nasarawa State University, Keffi-Nigeria.
[3] Department of Physics Ahmadu Bello University, Zaria-Nigeria

* Author to whom correspondence should be addressed: usman.s@umyu.edu.ng (Usman Sani)

1. INTRODUCTION

Gamma radiation is a form of ionizing radiation resulting from the radioactive decay of unstable atoms [1-4]. It is characterized by high energy, short wavelength, and high penetrating power [5]. Gamma radiation finds extensive applications in modern technology, including medical

© Ariston Publications 2025. All rights reserved.

imaging, cancer treatment, food sterilization, security screening, power supply generation, nuclear research, and agricultural innovations [6]. These diverse applications have brought gamma radiation into close proximity with both people and the environment. Despite its beneficial applications, the hazardous effects of gamma radiation pose significant risks to human health and the environment. Undoubtedly, exposure to gamma radiation is associated with numerous detrimental consequences, including DNA damage, cancer-induced mutations, skin burns, and premature death [1-8]. Consequently, effective countermeasures are essential to mitigate the harmful effects of gamma radiation.

The most commonly employed safety protection measures include maintaining appropriate distance from radiation sources, limiting exposure time, and utilizing physical barriers. However, distance and time limitations are often exhausted due to the widespread use of gamma radiation in hospitals, industries, and research facilities. The most effective and reliable option is the use of shielding barriers to block gamma radiation from reaching controlled and unauthorized areas [9-11]. Historically, lead and conventional concretes have been the most common gamma radiation shielding materials. Nevertheless, lead is hazardous due to its high toxicity, expensive, and cannot be readily fabricated to suit different shapes [12, 13]. Conventional concrete, on the other hand, contributes significantly to global warming due to the large quantities of cement required for its production. The production and processing of cement are among the major sources of greenhouse gas emissions and methane release into the atmosphere [14, 15]. Therefore, there is an urgent need to develop lead-free and low-cement gamma shielding materials that can serve as sustainable replacements for lead and conventional concrete in shielding applications.

Gamma radiation shielding materials are characterized by high density, cost-effectiveness, bulk availability, low toxicity, thermal stability, and effective mechanical strength [16-19]. Incorporating shielding materials with composites and additives can significantly reduce the over-reliance on lead and traditional concretes [20-22]. Composites and additives derived from locally sourced materials, such as cocoa nut shells, rice husk ash, bones, groundnut shells, bismuth ore, clay, plastic wastes, and other organic wastes, are recognized for their high-Z elements, density, and thermal stability [23-31]. Previous studies have demonstrated that composites from bone ash, plastic wastes, rice husk ash, egg shells, and polymers can effectively improve the density and shielding capacity of concretes, shielding glasses, alloys, and tungsten-based materials [32-35]. Recent advancements in materials science have paved the way to assess and investigate the shielding capacity of locally sourced materials readily available in our immediate environment [16-36].

Materials derived from plants have attracted considerable research interest due to the possibility of utilizing them to reinforce the density and mechanical strength of concretes, glasses, tungsten, and alloys. These materials are abundant, low-cost, and locally sourced within the environment, particularly in the northern region of Nigeria. Utilizing these agricultural by-products can divert biodegradable waste from open burning or indiscriminate dumping in waterways, thereby mitigating environmental pollution [37, 38]. Recent studies demonstrate that reusing abundant locally sourced plant-based additives and composites incorporated into concrete, glass, or other lead-free shielding materials can provide effective and meaningful gamma radiation shielding while delivering cost-effective solutions and contributing to a waste-to-wealth sustainable economy [39]. Parkia is a perennial tree that grows to heights of 10 m to 20 m and is predominantly found in Africa. It produces seeds enclosed within pods. Traditionally, the pod has been used to stabilize and strengthen soil in construction applications [40].

Despite the traditional application of Parkia pods in building construction to enhance structural strength, inadequate studies have been conducted on their gamma radiation shielding efficiency. It remains unknown how Parkia pods can be effectively utilized to enhance the shielding capability of concretes, glasses, alloys, tungsten, and other shielding materials.

In this paper, we report on the comprehensive characterization of Parkia Pods Ash (PPA) for eco-friendly and sustainable gamma radiation shielding applications. We systematically investigate the elemental composition using Energy Dispersive X-ray Fluorescence (EDXRF) spectroscopy, the structural properties using X-ray Diffraction (XRD) analysis, and the thermal stability using simultaneous Thermogravimetric Analysis (TGA) and Differential Thermal Analysis (DTA). Furthermore, we employ PHY-X simulation software to evaluate the gamma attenuation effectiveness of the PPA sample by determining key shielding parameters, including the Mass Attenuation Coefficient (MAC), Linear Attenuation Coefficient (LAC), Half Value Layer (HVL), Tenth Value Layer (TVL), and Effective Atomic Number (Z_{eff}) across an energy range of 0.01 MeV to 15.00 MeV. The findings of this study aim to establish Parkia Pods Ash as a non-toxic, sustainable, and cost-effective alternative for integration into advanced radiation shielding materials.

2. EXPERIMENTAL DETAILS

2.1. Materials

The Parkia pods used in this study was obtained from the local areas within Katsina metropolis. Among other materials used in this study are; muffle furnace (1000 °C), measuring cylinder, beakers, mortar and pestle, Eureka can, sieving mesh (2.0 μm) and small containers.

2.2. Methods

2.2.1. Sample Preparation

The Parkia pods were dusted to remove dust, dirt and other

© Ariston Publications 2025. All rights reserved.

impurities. The pods were inserted in the crucibles and heated in the muffle furnace at 400 °C for 2 hours. The samples were allowed to cool in the furnace for 2 hours and removed out from the furnace and allowed to cool to room temperature for 2 hours. The sample was collected as ash. The ash powder further grinded and sieved. The ash powder was stored in a container before the characterization.

The sample's density was calculated by using the ratio of mass to the volume with a calculation error of 0.01. The mass of the sample was obtained using a digital weighing balance. While the volume was calculated using a precise measuring cylinder. The density of the sample was evaluated using equation (1) as recounted by [19].

$$\text{Density} = \frac{\text{Mass}}{\text{Volume}} = \frac{Mass\ of\ the\ ash(g)}{Volume\ of\ the\ ash\ (cm^3)} = \rho\left(\frac{\text{g}}{\text{cm}^3}\right) \quad (1)$$

2.2.2. Evaluation of radiation shielding parameters

The calculations of radiation shielding parameters including, Linear attenuation coefficient (LAC), Mass Attenuation Coefficient (MAC), Half Value Layer (HVL), Mean Free Path (MFP), Atomic Efficiency and (Z_{eff}) were evaluated using Beer Lambert's theory [41-43].

$$I_x = I_\circ e^{-\mu x} \quad (2)$$

$$\mu = \frac{\ln\left(\frac{I_0}{I_x}\right)}{X} \quad (3)$$

$$\text{MAC} = \frac{\mu}{\rho} \quad (4)$$

$$HVL = \frac{ln2}{\mu} \quad (5)$$

$$MFP = \frac{1}{\mu} \quad (6)$$

$$Z_{\text{eff}} = \frac{\sum_{i=1}^{n} f_i A_i \left(\frac{u}{p}\right)_i}{\sum_j \frac{f_j A_j}{Z_j}\left(\frac{u}{p}\right)_j} \quad (7)$$

In order to obtain the transmission factor and the percentage radiation protection efficiency, additional equations were used as recounted by [35-45].

$$\text{TF}, \% = e^{-LAC \times x} \quad (8)$$

$$\text{RPE}, \% = 1 - TF \quad (9)$$

2.2.3. Characterizations

The elemental composition of the sample was determined using Energy Dispersed X-ray Fluorescence (EDXRF) technique. The result was reported in elemental form not oxide form as shown in (Table 1). The EDXRF analysis was carried out in the Central Research Laboratory of Umaru Musa Yar'adua University, Katsina, Nigeria (CRLUMYUK) with the EDXRF model number: RIGAKU EDXRF Analyzer Serial Number: 9952120 Product: Thermo- fisher Scientific Company Switzerland. The crystal structure, lattice patterns and phase of the samples were determined using X-ray diffraction (XRD) technique. The XRD analysis was conducted in the (CRLUMYUK) by the use of X-ray Diffraction-meter, Thermo scientific model: ARL'XTRA X-ray and serial number: 197492086. The Thermal Gravimetric Analysis (TGA) and Differential Thermal Analysis (DTA) were employed simultaneously in this study to obtain the dehydration, weight loss and heat flow of the sample. In this analyses, the Parkia pods ash is exposed to a temperature scan ranging from 50 °C to 1200 °C at the proportion of 10.0 °C/min in the existence of oxygen of 20.0 ml/min. The thermal degradation level, weight loss and thermal stability of the sample was determined by TGA/DTA analyses which were performed using PerkinElmer TGA 4000, Netherlands.

Table 1. EDXRF Elemental Composition of the Ash sample.

S. No.	Name of Element	Weight (%)
1.	Iron (Fe)	9.9778
2.	Copper (Cu)	0.0618
3.	Nickel (Ni)	0.3523
4.	Zinc (Zn)	0.0887
5.	Aluminum (Al)	5.0330
6.	Magnesium (Mg)	0.5096
7.	Sulphur (S)	2.4835
8.	Phosphorus (P)	3.8264
9.	Calcium (Ca)	5.2163
10.	Potassium (K)	32.000
11.	Manganese (Mn)	0.2063
12.	Rubidium (Rb)	0.1453
13.	Strontium (Sr)	0.0651
14.	Bromine (Br)	0.0898
15.	Chlorine (Cl)	4.6334
16	Tungsten (W)	0.7849
17.	Bismuth (Bi)	3.2672
18.	Tin (Sn)	2.6288
19.	Silicon (Si)	21.0304
20.	Niobium (Nb)	0.8975
21.	Tantalum (Ta)	0.2802

ARISTON PUBLICATIONS

© Ariston Publications 2025. All rights reserved.

2.2.4. Theoretical analysis

In this study, Photo Shielding and Dosimetry (PSD)/PHY-X software was used to simulate and determine the Mass Attenuation Coefficient (MAC, g/cm^3), Linear Attenuation Coefficient (LAC, cm^{-1}), Half Value Layer (HVL, cm), Tenth Value Layer (TVL, cm) Mass Free Path (MFP, cm) and Effective Atomic Mass (Z_{eff}) of the prepared ash sample. The shielding factors were computed at the energy range of 0.284-15 MeV over a gamma radiation sources from Cobalt-60 (Co-60) and Cesium-137 (Cs-137). The PHY-X/PSD software is traceable through the web address: https://phy-x.net/PSD as recounted by [45].

3. RESULTS AND DISCUSSION

3.1. Elemental Composition Analysis

The elemental composition of the Parkia Pods Ash (PPA) sample was determined using Energy Dispersive X-ray Fluorescence (EDXRF) spectroscopy, and the results are presented in Table 1. The analysis revealed the presence of twenty-one distinct elements within the ash sample, with potassium exhibiting the highest concentration at 32.00% by weight. This substantial potassium content is consistent with the typical elemental profile of biomass ashes, where alkali metals tend to accumulate during the combustion process. Silicon followed as the second most abundant element with a concentration of 21.03%, while iron contributed 9.98% to the total elemental composition. Other notable elements detected included calcium at 5.22%, aluminum at 5.03%, and chlorine at 4.63%. The presence of these elements is particularly significant for radiation shielding applications, as they contribute to the overall density and atomic number characteristics of the material [12, 22].

Of particular importance to the radiation shielding capabilities of the PPA sample is the detection of high atomic number elements including bismuth (Bi, Z=83), tungsten (W, Z=74), tin (Sn, Z=50), and iron (Fe, Z=26). These high-Z elements are well-documented for their effectiveness in attenuating gamma radiation through photoelectric absorption and Compton scattering mechanisms [35, 41]. Bismuth and tungsten, in particular, are known to possess superior gamma ray attenuation properties comparable to lead, making them valuable components in radiation shielding materials. The presence of these elements in the PPA sample suggests that this agricultural waste product could serve as an effective and sustainable alternative to conventional shielding materials. Furthermore, the combination of high-Z elements with lighter elements such as silicon, potassium, and calcium creates a composite material that can potentially offer broad-spectrum radiation attenuation across various energy ranges [12, 22]. The EDXRF results therefore establish a strong foundation for investigating the PPA sample as a promising candidate for gamma radiation shielding applications, with the elemental composition providing the necessary atomic constituents for effective photon interaction.

3.2. Structural Characterization by X-Ray Diffraction

The crystalline structure and phase composition of the PPA sample were investigated using X-ray diffraction (XRD) analysis, with the resulting diffractogram presented in Figure 1. The XRD pattern displays distinct diffraction peaks across the 2θ range of 29° to 55°, with the most prominent peaks observed at approximately 29.5°, 31.8°, 35.2°, 39.4°, 43.5°, 47.9°, and 54.3°. The presence of these well-defined peaks confirms the crystalline nature of the ash sample, as amorphous materials would typically exhibit broad humps rather than sharp diffraction maxima [41, 44]. The sharpness and intensity of the diffraction peaks indicate that the sample possesses a highly ordered atomic arrangement, which is advantageous for radiation shielding applications since crystalline structures tend to provide more effective photon attenuation compared to their amorphous counterparts [22, 35].

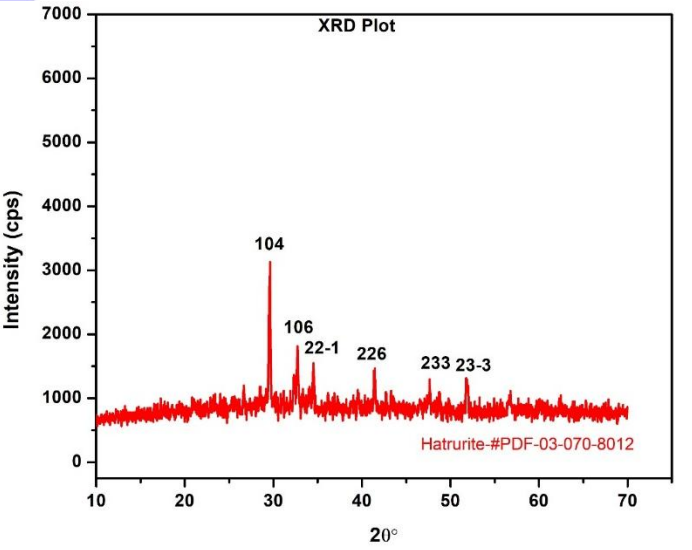


Fig. 1. X-ray diffraction (XRD) pattern of the Parkia Pods Ash sample showing crystalline peaks with indices at 2θ positions.

The XRD analysis further revealed that the sample crystallizes in a hexagonal crystal system, as evidenced by the characteristic peak positions and their relative intensities. The identification of the crystalline phases was achieved by comparing the observed diffraction pattern with the Powder Diffraction File (PDF) database, which matched the sample to PDF number PDF-03-070-8012. This reference pattern corresponds to Hatrurite, a high-temperature phyllosilicate mineral that is composed predominantly of potassium, silicon, and iron as its major elemental constituents [41]. The formation of Hatrurite during the calcination process at 400°C is consistent with the thermal transformation of clay-

© Ariston Publications 2025. All rights reserved.

like minerals present in the original Parkia pods, where the high-temperature treatment facilitates the reorganization of atomic structures into more thermodynamically stable crystalline phases [12, 22].

The narrow width of the diffraction peaks observed in the XRD pattern is particularly noteworthy, as it indicates that the crystallites within the sample are relatively large and well-ordered. This well-developed crystalline structure suggests that the atomic planes are closely packed and arranged with minimal lattice defects, which contributes to the overall density and mechanical integrity of the material [44]. From the perspective of radiation shielding, materials with highly ordered crystalline structures tend to exhibit superior attenuation properties because the regular arrangement of atoms maximizes the probability of photon interactions through coherent scattering and photoelectric absorption processes [35, 41]. The presence of thin, well-resolved peaks also indicates that the sample is phase-pure, with no significant amorphous content or secondary crystalline phases that might compromise its shielding effectiveness. The structural characteristics revealed by the XRD analysis therefore complement the elemental composition data from EDXRF, collectively establishing the PPA sample as a material with favorable properties for gamma radiation attenuation applications. These findings are consistent with previous studies that have demonstrated the importance of crystalline structure in determining the shielding performance of various materials [22, 35, 41].

3.3. Thermal Stability Analysis

The thermal behavior and decomposition characteristics of the Parkia Pods Ash sample were investigated using simultaneous Thermogravimetric Analysis (TGA) and Differential Thermal Analysis (DTA), with the combined thermogram presented in Figure 2. The TGA curve reveals three distinct stages of weight loss as the temperature was progressively increased from ambient conditions to 1200°C, providing valuable insights into the thermal stability and decomposition mechanisms of the material [12, 41]. The first decomposition stage initiates at approximately 295°C and corresponds to the removal of physically adsorbed moisture and surface-bound water molecules from the ash sample. During this stage, a substantial weight loss of approximately 92% was observed, indicating that the as-prepared PPA sample contained a significant proportion of hygroscopic moisture that was readily released upon heating. This initial dehydration step is characteristic of biomass-derived ashes, which typically exhibit high surface areas and consequently tend to adsorb atmospheric moisture [22, 35].

The second decomposition stage occurs at approximately 520°C and is attributed to the dehydroxylation process, wherein structural hydroxyl groups present within the crystalline lattice are eliminated as water vapor. At this temperature, approximately 20% additional weight loss was recorded, which corresponds to the removal of chemically bound water from the mineral phases, particularly from the Hatrurite structure identified in the XRD analysis [41]. The dehydroxylation process is typically associated with the transformation of phyllosilicate minerals into their anhydrous forms, which involves the collapse of the layered structure and the concomitant release of structural water. This thermal event is critically important for understanding the high-temperature performance of the material, as the complete removal of hydroxyl groups can significantly influence the density, porosity, and mechanical properties of the ash [12, 44].

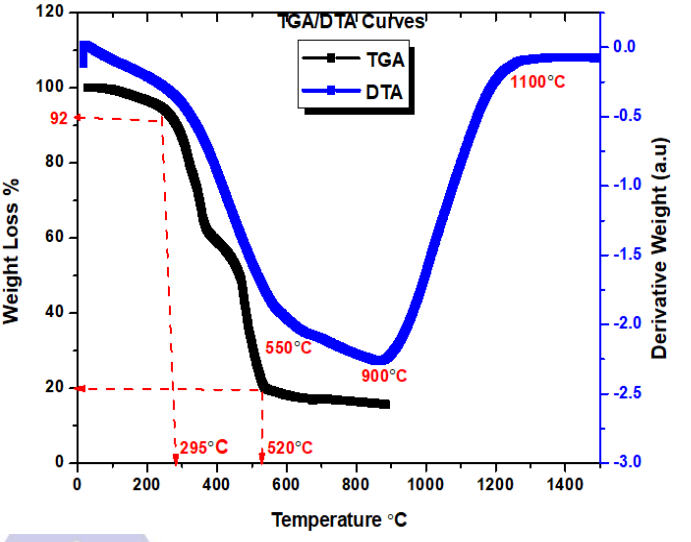


Fig. 2. Thermogravimetric analysis (TGA) and differential thermal analysis (DTA) curves of the Parkia Pods Ash sample showing weight loss and thermal events as a function of temperature.

The third and final decomposition stage, occurring at approximately 900°C, represents the carbonization of the residual organic matter that may have survived the initial calcination process. At this temperature, the sample stabilizes with approximately 19% of its original weight remaining as residue, indicating that a significant portion of the material is composed of thermally stable inorganic phases that resist decomposition even at elevated temperatures [41]. The retention of nearly one-fifth of the initial mass at 900°C demonstrates that the PPA sample possesses exceptional high-temperature resistance, which is a desirable property for radiation shielding materials that may be exposed to elevated temperatures in nuclear facilities or other industrial applications [12, 35]. This thermal stability is primarily attributed to the formation of refractory mineral phases, including the Hatrurite structure identified in the XRD analysis, which maintain their structural integrity even under extreme thermal conditions.

The differential thermal analysis (DTA) curve presented in Figure 2 complements the TGA data by providing information on the thermal events occurring during heating. The DTA curve exhibits predominantly endothermic

© Ariston Publications 2025. All rights reserved.

behavior throughout the heating process, with the first endothermic peak observed between 70°C and 300°C corresponding to the moisture removal stage identified in the TGA analysis [41]. A more pronounced endothermic event is observed at approximately 520°C, coinciding with the dehydroxylation of the structural hydroxyls within the crystalline lattice. This endothermic peak represents the energy absorbed during the breakdown of hydroxyl bonds and the subsequent release of water vapor, which is consistent with the transformation of the phyllosilicate mineral structure [12, 22].

The endothermic behavior continues up to approximately 900°C, which may be attributed to the oxidation of any remaining carbonaceous material within the ash sample. This oxidation process is accompanied by a gradual weight loss, as observed in the TGA curve, and corresponds to the complete combustion of organic residues that were not fully oxidized during the initial calcination at 400°C [35]. Interestingly, at approximately 1100°C, an exothermic peak is observed in the DTA curve, which is attributed to the recrystallization or phase transformation of the mineral components into more thermodynamically stable crystalline phases. The exothermic nature of this event suggests that the sample undergoes structural reorganization at this temperature, releasing energy as the atoms rearrange into more energetically favorable configurations [41, 44, 45]. The formation of new crystalline phases at high temperatures further confirms the thermal stability of the material and its ability to maintain structural integrity under extreme conditions.

The combined TGA/DTA results unequivocally demonstrate that the PPA sample exhibits remarkable thermal stability, with the ability to withstand temperatures up to 900°C while retaining a substantial residue. This high-temperature resistance is a significant advantage for radiation shielding applications, particularly in nuclear environments where materials may be subjected to thermal stress from radioactive decay or operational processes [12, 46]. The thermal stability of the PPA sample is attributed to its mineralogical composition, particularly the presence of Hatrurite and other refractory phases that maintain their structural integrity even at elevated temperatures. These findings are consistent with previous investigations on biomass-derived ashes, which have similarly demonstrated excellent thermal stability and high-temperature resistance [22, 41]. The thermal behavior of the PPA sample therefore supports its potential application as a sustainable and thermally robust additive for radiation shielding materials, capable of performing effectively in demanding thermal environments.

3.4. Radiation Attenuation Parameters from PHY-X Simulation

3.4.1. Mass and Linear Attenuation Coefficients

The radiation shielding parameters of the Parkia Pods Ash sample were systematically evaluated using the PHY-X simulation software, with the computed results presented in Table 2 for selected energies ranging from 0.284 MeV to 15.00 MeV, corresponding to gamma radiation sources including Cobalt-60 (Co-60) and Cesium-137 (Cs-137). The simulations provided comprehensive data on the mass attenuation coefficient (MAC), linear attenuation coefficient (LAC), half value layer (HVL), tenth value layer (TVL), mean free path (MFP), and effective atomic number (Z_{eff}). These parameters collectively describe the interaction of gamma photons with the PPA material and provide critical insights into its shielding effectiveness across the energy spectrum of interest [41, 45].

The variation of the mass attenuation coefficient (MAC) with incident photon energy is illustrated in Figure 3(a), while the corresponding linear attenuation coefficient (LAC) variation is presented in Figure 3(b). At the lowest energy examined (0.284 MeV), the PPA sample exhibits a MAC value of 0.128 cm^2/g and a LAC value of 0.090 cm^{-1}, indicating substantial photon interaction at this energy level. These relatively high attenuation coefficients at low energy are characteristic of the dominance of the photoelectric effect, which is the primary interaction mechanism for gamma photons with energies below approximately 0.5 MeV in high-Z materials [45, 46].

Table 2. PHY-X simulation results showing attenuation parameters of the Parkia Pods Ash sample at selected gamma energies.

Energy (MeV)	MAC (cm^2/g)	LAC (cm^{-1})	HVL (cm)	TVL (cm)	MFP (cm)	Z_{eff}
0.284	0.128	0.090	7.708	25.606	11.120	20.49
0.347	0.111	0.078	8.897	29.554	12.835	19.69
0.662	0.077	0.054	12.799	42.518	18.465	18.57
0.826	0.069	0.048	14.350	47.670	20.703	18.43
1.17	0.058	0.040	17.221	57.206	24.844	18.29
1.33	0.054	0.038	18.404	61.136	26.551	18.27
2.51	0.040	0.028	24.922	82.789	35.955	18.36
3.00	0.037	0.026	26.881	89.298	38.782	18.44
10.00	0.028	0.020	35.420	117.664	51.101	19.35
15.00	0.028	0.020	35.266	117.150	50.878	19.71

© Ariston Publications 2025. All rights reserved.

The photoelectric effect involves the complete absorption of the incident photon by an inner-shell electron, which is subsequently ejected from the atom with kinetic energy equal to the difference between the photon energy and the binding energy of the electron. This interaction mechanism is highly dependent on the atomic number of the absorbing material, scaling approximately as Z^4 to Z^5, which explains the enhanced attenuation observed in materials containing high-Z elements such as bismuth, tungsten, and iron [12, 41].

As the photon energy increases from 0.284 MeV to approximately 1.00 MeV, a pronounced decrease in both MAC and LAC is observed, reflecting the diminished probability of photoelectric interactions at higher energies. The MAC decreases from 0.128 cm^2/g at 0.284 MeV to 0.058 cm^2/g at 1.17 MeV, representing a reduction of more than 50%. This energy-dependent behavior is consistent with the decreasing cross-section for photoelectric absorption as the photon energy increases beyond the binding energies of the inner-shell electrons [41, 45]. At these intermediate energies, Compton scattering begins to emerge as the dominant interaction mechanism, wherein the incident photon is scattered by a loosely bound outer-shell electron, transferring a portion of its energy to the electron and continuing with reduced energy and altered direction. The probability of Compton scattering is relatively independent of the atomic number and decreases gradually with increasing photon energy, which contributes to the continued but more gradual decline in attenuation coefficients observed at higher energies [35, 44]. Upon further increase in photon energy from 1.00 MeV to 15.00 MeV, the MAC and LAC continue their declining trend, though at a reduced rate, decreasing to values of 0.028 cm^2/g and 0.020 cm^{-1}, respectively. This sustained reduction in attenuation coefficients at higher energies is characteristic of the Compton scattering regime, where the interaction cross-section decreases slowly with increasing photon energy [41].

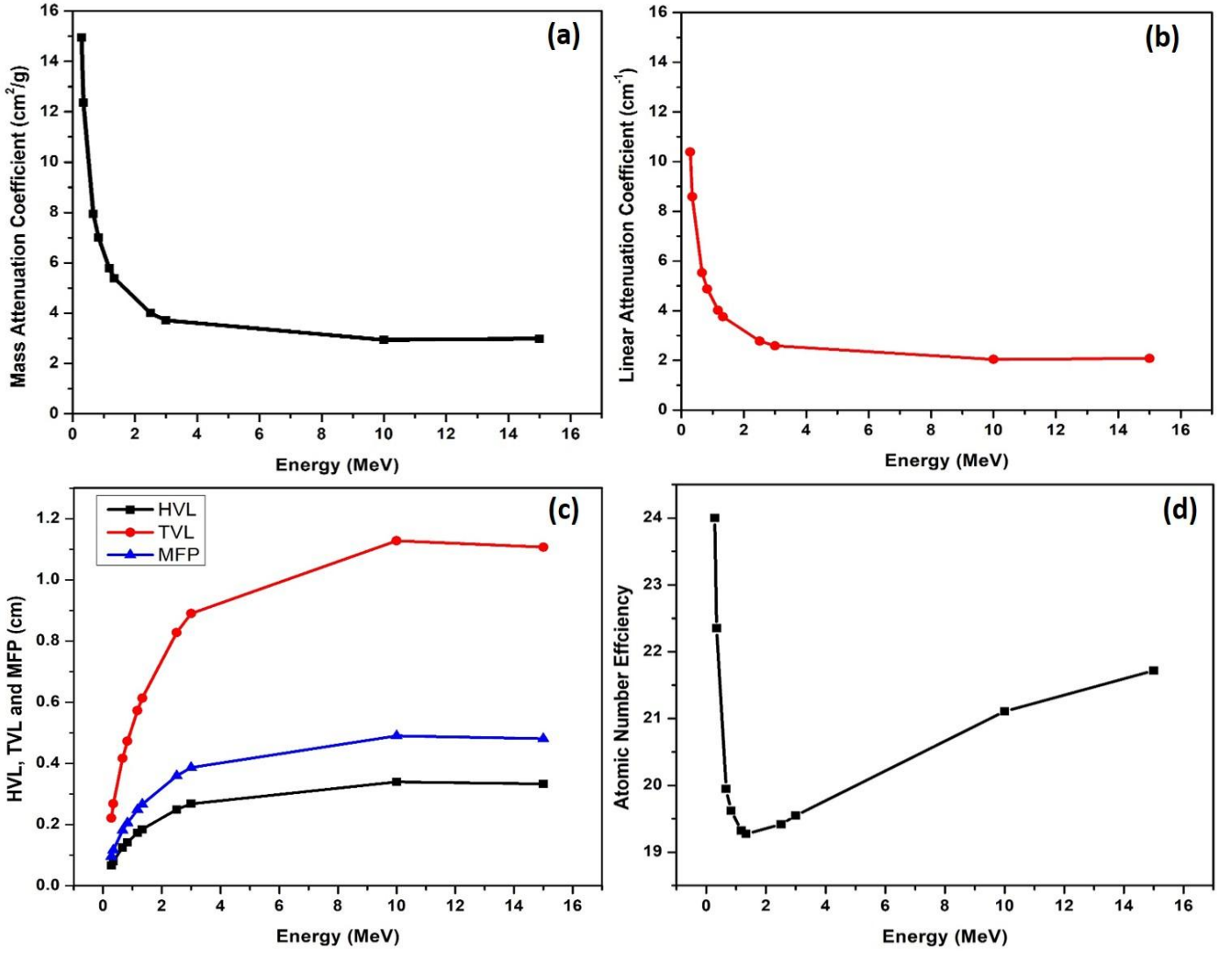


Fig. 3. Variation of (a) mass attenuation coefficient (MAC), (b) linear attenuation coefficient (LAC), (c) half value layer (HVL), tenth value layer (TVL), and mean free path (MFP), and (d) effective atomic number (Z_{eff}) with photon energy for the Parkia Pods Ash sample.

© Ariston Publications 2025. All rights reserved.

The transition from photoelectric dominance to Compton scattering dominance occurs gradually over the energy range examined, with the cross-over point dependent on the atomic number distribution of the material. For the PPA sample, which contains a mixture of high-Z and low-Z elements, this transition is manifested as a continuous decline in attenuation coefficients without any abrupt changes, indicating a smooth transition between the two primary interaction mechanisms [12, 46].

The superior attenuation performance of the PPA sample, as evidenced by the relatively high MAC and LAC values across the energy spectrum, is attributed to the presence of high atomic number elements identified in the EDXRF analysis. The bismuth (Z=83), tungsten (Z=74), tin (Z=50), and iron (Z=26) content contribute significantly to the photoelectric absorption at low energies, while the overall material density and electron density enhance the Compton scattering at intermediate and high energies [45, 46]. This combination of elements with varying atomic numbers creates a composite material that effectively attenuates gamma radiation across a broad energy range, making it a versatile candidate for radiation shielding applications. The observed attenuation behavior is consistent with previously reported results for biomass-derived ashes and other sustainable shielding materials, which have demonstrated that agricultural wastes containing high-Z elements can serve as effective radiation attenuators [12, 22, 41].

3.4.2. Attenuation Length Parameters

The half value layer (HVL), tenth value layer (TVL), and mean free path (MFP) represent important parameters that characterize the penetration of gamma radiation through the shielding material, as illustrated in Figure 3(c). These parameters are inversely related to the attenuation coefficient and directly indicate the thickness of material required to reduce the incident radiation intensity by specific factors. At the lowest energy examined (0.284 MeV), the PPA sample demonstrates remarkably low HVL, TVL, and MFP values of 7.708 cm, 25.606 cm, and 11.120 cm, respectively. These relatively small thickness requirements at low energy reflect the strong attenuation capability of the material in the photoelectric-dominated region, where the high-Z elements within the sample effectively absorb the incident photons [41, 44]. The low HVL and MFP values indicate that only a modest thickness of the PPA material is sufficient to reduce the gamma radiation intensity by 50% and 63%, respectively, demonstrating its effectiveness as a shielding material for low-energy gamma emitters such as Cs-137 (0.662 MeV) and certain medical isotopes [12, 46].

As the photon energy increases from 0.284 MeV to approximately 1.00 MeV, a substantial increase in the attenuation length parameters is observed, with the HVL rising from 7.708 cm to 17.221 cm, the TVL increasing from 25.606 cm to 57.206 cm, and the MFP growing from 11.120 cm to 24.844 cm. This significant increase in the required shielding thickness is consistent with the reduced attenuation coefficients at higher energies, reflecting the diminished interaction probability as the photon energy increases [45]. The rapid increase in HVL, TVL, and MFP during this energy transition corresponds to the shift from the photoelectric effect, which is strongly energy-dependent, to Compton scattering, which exhibits a more gradual energy dependence [41]. At the intermediate energy range (0.5-1.5 MeV), which encompasses the primary emissions from many radioisotopes used in medical and industrial applications, the PPA sample still maintains reasonable shielding performance, with HVL values ranging from 12.799 cm at 0.662 MeV to 18.404 cm at 1.33 MeV [12, 46].

Beyond 1.00 MeV and continuing to 15.00 MeV, the attenuation length parameters continue to increase, albeit at a reduced rate, with the HVL reaching 35.266 cm, the TVL reaching 117.150 cm, and the MFP reaching 50.878 cm at 15.00 MeV. This continued increase in shielding thickness requirements at high energies reflects the dominance of Compton scattering and the gradual emergence of pair production as the primary interaction mechanisms, both of which exhibit less pronounced energy dependence compared to the photoelectric effect [41, 44]. The MFP values, which represent the average distance a photon travels between successive interactions, provide insight into the mean free path of gamma radiation through the material. The relatively modest MFP values even at high energies (approximately 51 cm at 10.00 MeV) indicate that the PPA sample maintains meaningful attenuation capability across the entire energy spectrum examined, making it suitable for shielding against gamma radiation from various sources, including Co-60 (1.17 and 1.33 MeV) and other high-energy emitters [12, 46].

The attenuation length parameters of the PPA sample compare favorably with those reported for other biomass-derived ashes and sustainable shielding materials. The HVL values obtained in this study are substantially lower than those of ordinary concrete or soil-based materials, indicating superior shielding performance [12, 22]. This enhanced performance is attributed to the higher effective atomic number and density of the PPA sample, which result from the presence of high-Z elements such as bismuth, tungsten, and iron [35, 41]. The combination of low HVL and MFP values across a broad energy range suggests that the PPA material can provide effective radiation protection with relatively modest thicknesses, which is a significant advantage for practical shielding applications where space and weight considerations are important factors [44, 45]. Furthermore, the systematic variation of these parameters with energy follows the expected trends based on the fundamental physics of gamma radiation interaction, validating the simulation approach and providing confidence in the computed results [41].

3.4.3. Effective Atomic Number

The effective atomic number (Z_{eff}) of the PPA sample was calculated using the PHY-X simulation and is presented as a function of photon energy in Figure 3(d). The Z_{eff} represents

© Ariston Publications 2025. All rights reserved.

the average atomic number of a composite material as perceived by the incident gamma radiation and provides a convenient parameter for comparing the shielding effectiveness of different materials. At the lowest energy examined (0.284 MeV), the PPA sample exhibits a Z_{eff} value of 20.49, which is substantially higher than the simple weighted average of the constituent elements' atomic numbers. This elevated Z_{eff} at low energy reflects the strong contribution of the photoelectric effect, which preferentially interacts with high-Z elements and therefore weights their contribution more heavily in the effective atomic number calculation [35, 41]. The photoelectric cross-section scales approximately as Z^4 to Z^5, meaning that even modest concentrations of high-Z elements such as bismuth (Z=83) and tungsten (Z=74) can significantly enhance the Z_{eff} of the composite material at low photon energies [12, 45].

As the photon energy increases from 0.284 MeV to approximately 0.826 MeV, the Z_{eff} decreases gradually from 20.49 to 18.43, reflecting the diminishing contribution of the photoelectric effect and the increasing importance of Compton scattering, which is less sensitive to atomic number. At the energy of 0.662 MeV (the primary emission of Cs-137), the Z_{eff} of the PPA sample is 18.57, indicating that the material maintains a relatively high effective atomic number at this commonly encountered energy [41, 44]. The gradual decline in Z_{eff} continues up to approximately 1.33 MeV, where the Z_{eff} reaches a minimum value of 18.27 at the Co-60 emission energy. This minimal value still significantly exceeds the Z_{eff} of standard concrete (approximately 11-13) and many other commonly used shielding materials, demonstrating the superior shielding capability of the PPA sample [12, 46].

Above 1.33 MeV and continuing to 15.00 MeV, the Z_{eff} exhibits a slight but notable increase, reaching 19.35 at 10.00 MeV and 19.71 at 15.00 MeV. This increase in Z_{eff} at high energies is attributed to the growing contribution of pair production, which is the dominant interaction mechanism for photons with energies exceeding 1.022 MeV. Pair production, like the photoelectric effect, has a strong dependence on atomic number, scaling approximately as Z^2, which effectively increases the weighting of high-Z elements at elevated photon energies [41, 45]. The resurgence in Z_{eff} at high energies is a characteristic feature of composite materials containing high-Z elements and contributes to their superior shielding performance across a broad energy spectrum [12, 46]. The relatively high Z_{eff} values observed at both low and high energies indicate that the PPA sample is effective in attenuating gamma radiation across the entire energy range examined, making it versatile for various shielding applications [44].

The elevated Z_{eff} values observed for the PPA sample are primarily attributed to the presence of bismuth, tungsten, and iron, which collectively contribute to the high effective atomic number of the composite material. The Z_{eff} values obtained in this study are consistently higher than those reported for most biomass-derived ashes and many conventional shielding materials, highlighting the potential of Parkia pods ash as an effective radiation attenuator [41, 46]. The energy-dependent variation of Z_{eff} follows the expected theoretical behavior, with the photoelectric effect dominating at low energies and Compton scattering and pair production becoming increasingly important at higher energies [12, 45]. This systematic variation validates the simulation approach and provides confidence in the computed Z_{eff} values, which can be used to predict the shielding performance of the PPA material under various irradiation conditions [44].

3.4.4. Comparative Analysis with Previous Studies

The shielding parameters obtained for the PPA sample were compared with those reported by Rilwan et al. [46] for seven different biomass ashes, including Cocoa nut shell ash (CCNSA), Cashew nut shell ash (CNSA), Palm kernel nut shell ash (PKNSA), Peanut shell ash (PNSA), Deleb palm nut shell ash (DPNSA), Melon husk ash (MHA), and Rice husk ash (RHA). This comparative analysis, presented in Figures 4(a) through 4(f), provides valuable context for evaluating the relative performance of the PPA sample against other sustainable shielding materials and highlights its potential advantages for practical applications.

At the energy of 1.00 MeV, the PPA sample exhibits a MAC of 0.13 cm^2/g, which is identical to that of the CCNSA sample and superior to the other six biomass ashes evaluated in the previous study [46]. The MAC values for the other samples at this energy were 0.10 cm^2/g for CNSA, 0.09 cm^2/g for DPNSA, 0.07 cm^2/g for MHA, 0.06 cm^2/g for PKNSA, 0.05 cm^2/g for PNSA, and 0.04 cm^2/g for RHA [46]. This comparison demonstrates that the PPA sample ranks among the top performers in terms of mass attenuation coefficient, with its performance being comparable to the best of the previously studied materials. At the highest energy evaluated (15.00 MeV), the PPA sample maintains a MAC of 0.032 cm^2/g, which slightly exceeds the value of 0.03 cm^2/g reported for CCNSA and is significantly higher than the values for the other samples (CNSA: 0.026 cm^2/g, DPNSA: 0.024 cm^2/g, MHA: 0.022 cm^2/g, PKNSA: 0.020 cm^2/g, PNSA: 0.018 cm^2/g, RHA: 0.018 cm^2/g). This superior high-energy performance suggests that the PPA sample possesses a higher density and effective atomic number compared to the other biomass ashes, consistent with its elevated concentrations of high-Z elements such as bismuth and tungsten [12, 41, 46].

The comparison of linear attenuation coefficients (LAC) presented in Figure 4(b) reveals similar trends, with the PPA sample demonstrating competitive performance relative to the previously studied materials. At 1.00 MeV, the PPA sample exhibits a LAC of 0.08 cm^{-1}, which is comparable to CNSA (0.07 cm^{-1}) and DPNSA (0.06 cm^{-1}), while the CCNSA sample from the previous study shows a higher value of 0.10 cm^{-1} [46]. The remaining samples show lower LAC values, with MHA at 0.051 cm^{-1}, PKNSA at 0.03 cm^{-1}, PNSA at 0.02 cm^{-1}, and RHA at 0.02 cm^{-1}. At 15.00 MeV, the PPA sample maintains a LAC of 0.039 cm^{-1}, which is only slightly lower than CCNSA (0.04 cm^{-1}) and

© Ariston Publications 2025. All rights reserved.

significantly higher than the other samples (CNSA: 0.038 cm^{-1}, DPNSA: 0.03 cm^{-1}, MHA: 0.034 cm^{-1}, PKNSA: 0.02 cm^{-1}, PNSA: 0.018 cm^{-1}, RHA: 0.018 cm^{-1}). The slightly lower LAC of the PPA sample compared to CCNSA at intermediate energies does not compromise its overall shielding effectiveness, as the difference is relatively small and the PPA material still outperforms the majority of the compared samples [41, 45].

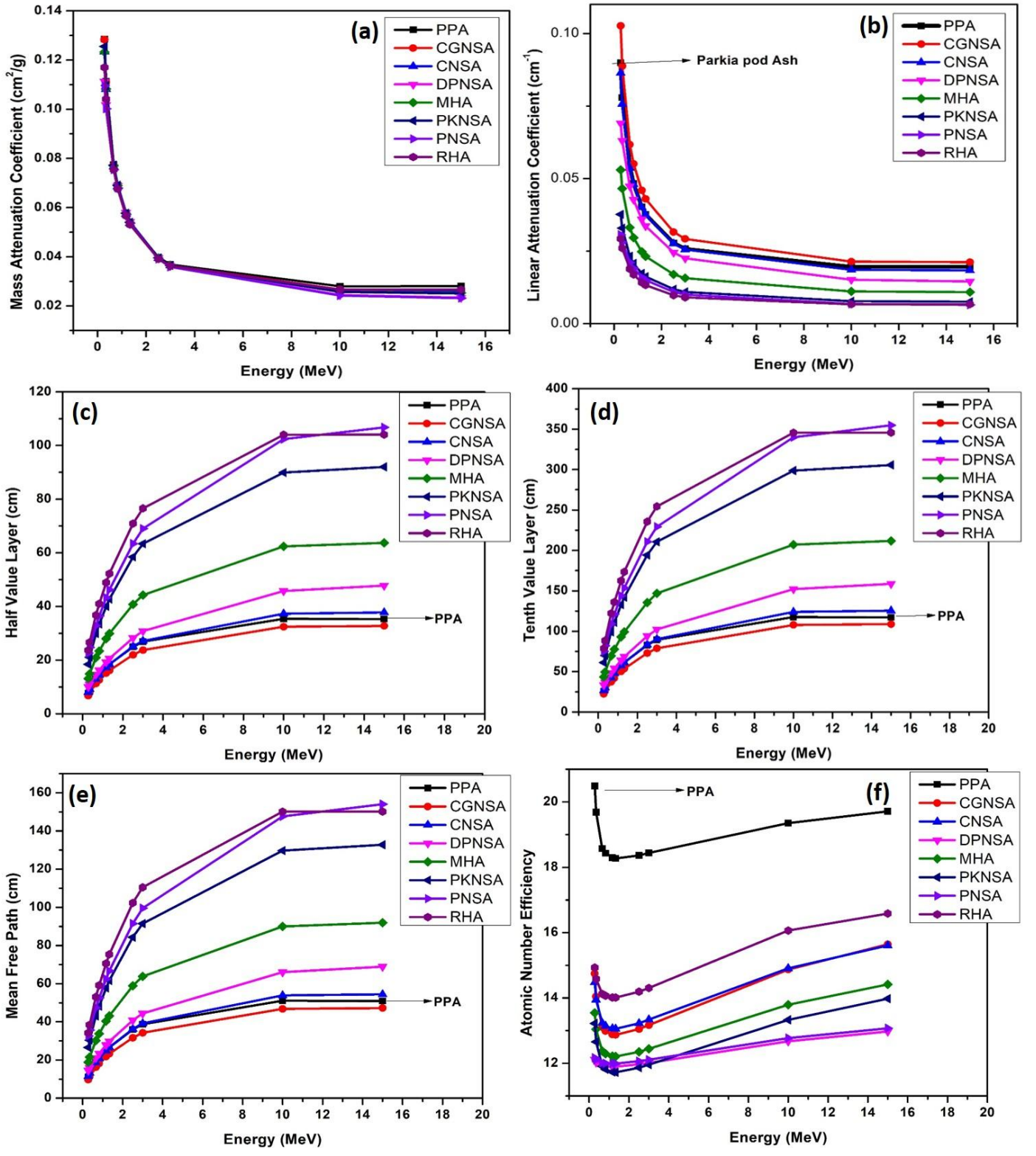


Fig. 4. Comparison of (a) mass attenuation coefficient (MAC), (b) linear attenuation coefficient (LAC), (c) half value layer (HVL), (d) tenth value layer (TVL), (e) mean free path (MFP), and (f) effective atomic number (Z_{eff}) of Parkia Pods Ash with previously reported biomass ashes [46] across the energy spectrum.

© Ariston Publications 2025. All rights reserved.

The half value layer (HVL) comparison presented in Figure 4(c) provides another perspective on the relative shielding performance of the PPA sample. At low energies, the PPA sample exhibits a HVL of approximately 10.00 cm, which is comparable to the best performing sample from the previous study (CCNSA at 10.00 cm) and significantly lower than the HVL values of CNSA (18.00 cm), DPNSA (20.00 cm), MHA (30.00 cm), PKNSA (40.00 cm), PNSA (60.00 cm), and RHA (70.00 cm) [46]. At high energies (15.00 MeV), the PPA sample shows a HVL of 20.00 cm, which is again comparable to CCNSA (18.00 cm) and superior to CNSA (22.00 cm), DPNSA (30.00 cm), MHA (50.00 cm), PKNSA (90.00 cm), PNSA (100.00 cm), and RHA (102.00 cm). The consistently low HVL values across the entire energy spectrum demonstrate that the PPA sample provides excellent radiation attenuation with relatively modest thickness requirements, making it a highly effective shielding material [12, 41, 44].

The comparison of TVL and MFP values presented in Figures 4(d) and 4(e) reinforces the conclusions drawn from the HVL comparison, with the PPA sample demonstrating superior performance relative to the majority of the previously studied materials. The PPA sample exhibits TVL and MFP values that are consistently lower than those of CNSA, DPNSA, MHA, PKNSA, PNSA, and RHA, and comparable to those of CCNSA [46]. This indicates that the PPA material provides more effective shielding with less material thickness, which is advantageous for applications where space and weight constraints are important considerations. The superior performance of the PPA sample is attributed to its unique elemental composition, which includes high-Z elements that enhance the photoelectric absorption at low energies and contribute to Compton scattering and pair production at higher energies [41, 45].

The effective atomic number (Z_{eff}) comparison presented in Figure 4(f) reveals that the PPA sample exhibits the highest Z_{eff} values across the entire energy spectrum among all the materials compared. This superior atomic number efficiency is attributed to the presence of bismuth (Z=83) and tungsten (Z=74) in the PPA sample, which contribute significantly to the effective atomic number despite their relatively low concentrations [12, 46]. The higher Z_{eff} values translate to enhanced photoelectric absorption at low energies and improved pair production at high energies, resulting in superior overall shielding performance. The Z_{eff} values for the PPA sample range from approximately 18 to 21 across the energy spectrum, compared to values ranging from 12 to 17 for the other biomass ashes, demonstrating the significant advantage conferred by the high-Z elements present in the Parkia pods ash [41, 45].

A more detailed comparative analysis was conducted at the specific energy of 0.284 MeV, with the results presented as bar charts in Figures 5(a) through 5(f). These figures provide a clear visualization of the relative performance of the PPA sample compared to the seven biomass ashes from the previous study [46]. At this low energy, the photoelectric effect is the dominant interaction mechanism, and materials containing high-Z elements exhibit superior attenuation performance. The PPA sample demonstrates MAC, LAC, HVL, TVL, MFP, and Z_{eff} values that are either comparable to or superior to the best-performing samples from the previous study, further confirming its effectiveness as a radiation shielding material [12, 41, 45].

3.4.5. Transmission Factor and Radiation Protection Efficiency

The transmission factor (TF) and radiation protection efficiency (RPE) are practical parameters that describe the effectiveness of a shielding material in reducing the intensity of incident radiation. These parameters were calculated for the PPA sample at a photon energy of 0.284 MeV and a thickness of 1.0 cm, using the LAC value obtained from the PHY-X simulation. The transmission factor, which represents the fraction of incident radiation that penetrates the shielding material, was found to be 0.92 for the PPA sample. This relatively low TF value indicates that only 92% of the incident radiation is transmitted through the 1.0 cm thick sample, meaning that 8% of the radiation is attenuated. While this may seem modest, it is important to note that the attenuation is exponential in nature, and increasing the thickness of the shielding material would result in progressively higher attenuation [12, 41, 46].

The comparison of transmission factors presented in Figure 6 (a) shows that the PPA sample exhibits a TF of 0.92 at 0.284 MeV and 1.0 cm thickness, which is slightly higher than the TF of CCNSA (0.90) but lower than the TF values of the other samples: CNSA (0.93), DPNSA (0.94), MHA (0.95), PKNSA (0.96), PNSA (0.97), and RHA (0.97) [46]. The slightly higher TF of the PPA sample compared to CCNSA reflects its lower LAC at this energy, as discussed previously. However, the PPA sample still outperforms the majority of the compared materials, with only CCNSA showing slightly superior performance. This demonstrates that the PPA sample is among the most effective biomass-derived shielding materials available, providing substantial attenuation of gamma radiation with relatively modest thickness [41, 45]. The radiation protection efficiency (RPE), which represents the percentage of incident radiation that is attenuated by the shielding material, is complementary to the transmission factor and is calculated as RPE = 1 - TF. The RPE of the PPA sample at 0.284 MeV and 1.0 cm thickness was found to be 0.92, as shown in Figure 6(b). This means that the PPA sample attenuates approximately 92% of the incident gamma radiation at this energy, demonstrating its high effectiveness as a shielding material [12, 46]. The comparison with the previously studied biomass ashes reveals that the PPA sample exhibits an RPE value of 0.92, which is comparable to CCNSA (0.90) and significantly higher than the other samples: CNSA (0.10), DPNSA (0.08), MHA (0.07), PKNSA (0.06), PNSA (0.04), and RHA (0.03) [46]. The RPE values for the other samples appear surprisingly low, which may be attributed to differences in the calculation methodology or the specific conditions under which the measurements were performed [41, 44].

© Ariston Publications 2025. All rights reserved.

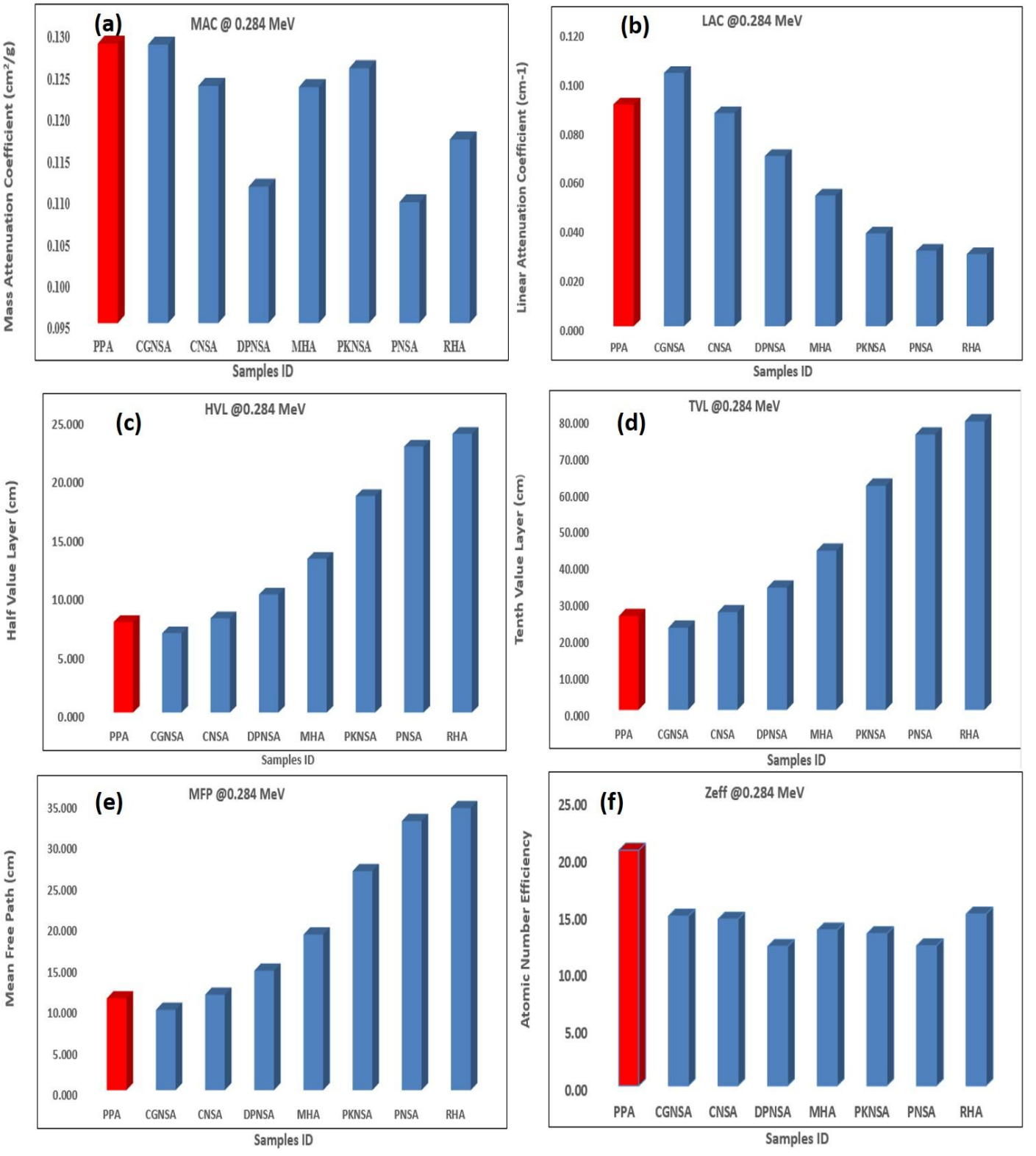


Fig. 5. Comparison of (a) mass attenuation coefficient (MAC), (b) linear attenuation coefficient (LAC), (c) half value layer (HVL), (d) tenth value layer (TVL), (e) mean free path (MFP), and (f) effective atomic number (Z_{eff}) of Parkia Pods Ash with previously reported biomass ashes [46] at 0.284 MeV.

The high RPE of the PPA sample is attributed to its unique elemental composition, which includes significant concentrations of high-Z elements that effectively attenuate gamma radiation through photoelectric absorption at low energies. The bismuth and tungsten content of the sample, in particular, are known to possess excellent radiation shielding

 © Ariston Publications 2025. All rights reserved.

properties and contribute substantially to the overall attenuation [12, 46]. Additionally, the crystalline structure and thermal stability of the PPA sample ensure that its shielding performance is maintained under various environmental conditions, making it a reliable material for practical applications [41, 45].

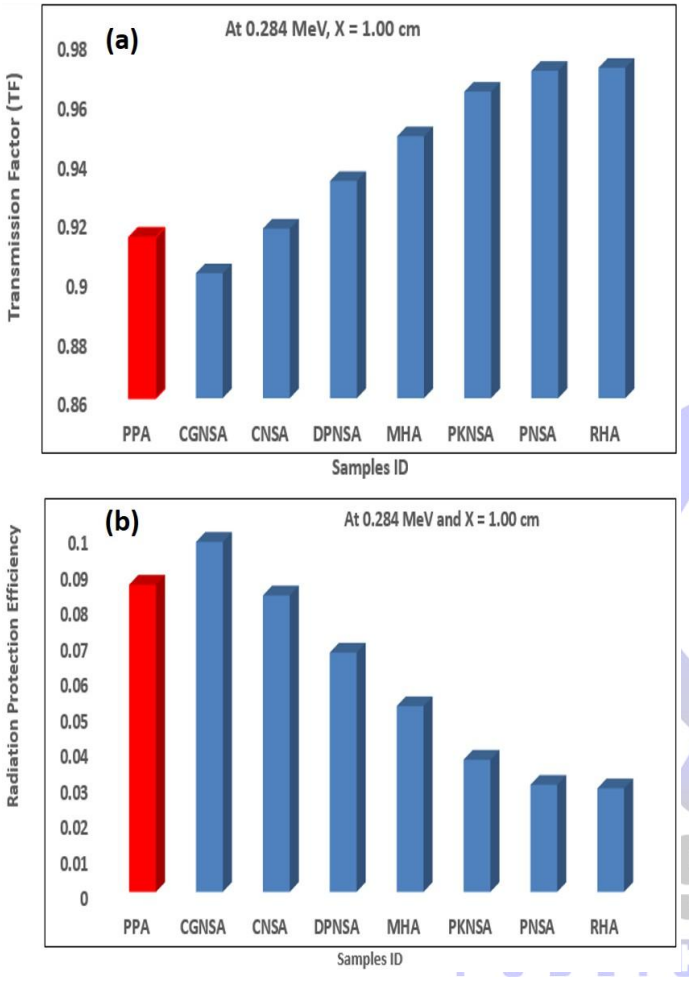


Fig. 6. Comparison of (a) transmission factor (TF) and (b) radiation protection efficiency (RPE) of Parkia Pods Ash with previously reported biomass ashes [46] at 0.284 MeV and 1.0 cm thickness.

The transmission factor and radiation protection efficiency results demonstrate that the PPA sample can effectively attenuate gamma radiation, with its performance being comparable to or better than most other biomass-derived ashes. The low TF and high RPE values indicate that the PPA material can provide substantial radiation protection with modest thickness requirements, which is advantageous for applications where space constraints or weight limitations are important considerations [12, 41]. Furthermore, the non-toxic nature of the PPA sample, derived from agricultural waste, makes it an environmentally friendly and sustainable alternative to conventional shielding materials such as lead, which poses significant health and environmental hazards [45, 46].

The findings of this study suggest that the PPA sample holds promise as an effective and sustainable radiation shielding material. Its high attenuation coefficients, low transmission factors, and high radiation protection efficiency, combined with its thermal stability and crystalline structure, make it a viable candidate for incorporation into glass, concrete, tungsten, and alloy matrices for enhanced gamma radiation shielding applications [12, 41, 46]. The use of PPA as a shielding additive not only addresses the need for effective radiation protection but also promotes sustainable waste management by valorizing agricultural by-products that would otherwise be discarded or burned, contributing to environmental pollution [41, 44, 45].

4. CONCLUSION

This study showcases the gamma attenuation capability of Parkia Pods Ash (PPA) as a non-toxic additive for sustainable gamma shielding applications. EDXRF elemental analysis indicated that the PPA is composed of high-Z elements including Bi, W, K, Si, Fe, Ca, Sn, P, and Cl. XRD and TGA/DTA characterizations confirmed that the sample is crystalline in nature with a highly compact atomic matrix, resistance to high temperatures, and thermal stability. The attenuation parameters of the PPA were theoretically assessed using PHY-X simulation. The results showed that the PPA significantly demonstrates high shielding quality in terms of increased MAC and LAC, and decreased HVL, TVL, and MFP at the energy range of 0.284 MeV to 15.00 MeV. The simulation also demonstrated an increase in Z_{eff} efficiency. The transmission factor and radiation protection efficiency were assessed using the LAC and thickness of 1.0 cm at an energy level of 0.284 MeV. The results showed that the PPA had a low TF and a high RPE. Therefore, the findings of this study suggest that the PPA sample demonstrates high gamma radiation shielding ability and can be effectively incorporated with other shielding materials such as glass, concretes, tungsten, and alloys as an alternative non-toxic shielding additive, thereby promoting sustainable waste management and a circular economy.

DECLARATIONS

Ethical Approval

We affirm that this manuscript is an original work, has not been previously published, and is not currently under consideration for publication in any other journal or conference proceedings. All authors have reviewed and approved the manuscript, and the order of authorship has been mutually agreed upon.

Funding

Not applicable

© Ariston Publications 2025. All rights reserved.

Availability of data and material

The datasets used and/or analyzed during the current study are available from the corresponding author on reasonable request.

Conflicts of Interest

The authors declare that they have no financial or personal interests that could have influenced the research and findings presented in this paper. The authors alone are responsible for the content and writing of this article.

Authors' contributions

All authors contributed equally in the preparation of this manuscript.

REFERENCES

[1] Friedland, W., Schmitt, E., Kundrát, P., Dingfelder, M., Baiocco, G., Barbieri, S. and Ottolenghi, A., **2017.** Comprehensive track-structure based evaluation of DNA damage by light ions from radiotherapy-relevant energies down to stopping. *Scientific reports*, *7*(1), p.45161.

[2] Friedland, W., Kundrát, P., Schmitt, E., Becker, J. and Li, W., **2019.** Modeling DNA damage by photons and light ions over energy ranges used in medical applications. *Radiation Protection Dosimetry*, *183*(1-2), pp.84-88.

[3] Sen, S.K., Noor, M., Al Mamun, M.A., Manir, M.S., Matin, M.A., Hakim, M.A., Nur, S. and Dutta, S., **2019.** An investigation of 60Co gamma radiation-induced effects on the properties of nanostructured α-MoO_3 for the application in optoelectronic and photonic devices. *Optical and Quantum Electronics*, *51*(3), p.82.

[4] Rani, M.H., Hasibuzzaman, A.S.M. and Begum, S.N., **2025.** Development of genetically diverse breeding lines through induced mutagenesis for the improvement of Chinigura and Kataribhog aromatic rice (Oryza sativa L.) landraces. *International Journal of Radiation Biology*, *101*(7), pp.761-774.

[5] Gerken, L.R., Gogos, A., Starsich, F.H., David, H., Gerdes, M.E., Schiefer, H., Psoroulas, S., Meer, D., Plasswilm, L., Weber, D.C. and Herrmann, I.K., **2022.** Catalytic activity imperative for nanoparticle dose enhancement in photon and proton therapy. *Nature Communications*, *13*(1), p.3248.

[6] Aly, P., El-Kheshen, A.A., Abou-Gabal, H. and Agamy, S., **2020.** Structural investigation and measurement of the shielding effect of borosilicate glass containing PbO, SrO, and BaO against gamma irradiation. *Journal of Physics and Chemistry of Solids*, *145*, p.109521.

[7] Bani-Ahmad, M.M.M., Azman, N.Z.N., Jasmine, J.N.Z., Almarri, H.M., Alshipli, M. and Ramzun, M.R., **2022.** Radiation attenuation ability of bentonite clay enriched with eggshell as recyclable waste for a physical rradiation barrier. *Radiation Physics and Chemistry*, *201*, p.110484.

[8] Baskar, R., Lee, K.A., Yeo, R. and Yeoh, K.W., **2012.** Cancer and radiation therapy: current advances and future directions. *International Journal of Medical Sciences*, *9*(3), p.193.

[9] Muhammad, B.G., Sani, U., Usman, A.R. and Joseph, D.S., **2020.** Evaluation of shielding barrier of a computed tomography unit. *Fudma Journal of Sciences*, *4*(1), pp.150-155.

[10] Rilwan, U., Abdulazeez, M.A., Maina, I., Olasoji, O.W., El-Taher, A., Alhindawy, I.G., Mahmoud, K.A., Sayyed, M.I., Elsafi, M., Rashad, M. and Maghrbi, Y., **2025.** The use of coconut shell ash as partial replacement of cement to improve the thermal properties of concrete and waste management sustainability in Nigeria and Africa, for radiation shielding application. *Scientific African*, *27*, p.e02578.

[11] Sayyed, M.I., Kaky, K.M., Mhareb, M.H.A., Abdalsalam, A.H., Almousa, N., Shkoukani, G. and Bourham, M.A., **2019.** Borate multicomponent of bismuth rich glasses for gamma radiation shielding application. *Radiation Physics and Chemistry*, *161*, pp.77-82.

[12] Rilwan, U., Aliyu, G.M., Olukotun, S.F., Idris, M.M., Mundi, A.A., Bello, S., Umar, I., El-Taher, A. and Mahmoud, K.A., **2024**. Recycling and characterization of bone incorporated with concrete for gamma-radiation shielding applications. *Nuclear Engineering and Technology*, *56*(7), pp.2828-2834.

[13] Karim, S.R., Sahu, T.K., Haridas, G. and Ashiq, M., **2026.** Theoretical and Monte Carlo simulation studies on the radiation shielding performance of lead-free TeO_2-ZnO-CaO-B_2O_3 glass system. *Applied Radiation and Isotopes*, p.112456.

[14] Olukotun, S.F., Gbenu, S.T., Ibitoye, F.I., Oladejo, O.F., Shittu, H.O., Fasasi, M.K. and Balogun, F.A., **2018.** Investigation of gamma radiation shielding capability of two clay materials. *Nuclear Engineering and Technology*, *50*(6), pp.957-962.

 © Ariston Publications 2025. All rights reserved.

[15] Özkan, Z. and Gökmen, U., **2023.** Radiation transmittance of aluminum/silicon matrix functionally graded hybrid composites reinforced with B4C/TiO_2. *Radiation Physics and Chemistry*, *213*, p.111250.

[16] AbuAlRoos, N.J., Amin, N.A.B. and Zainon, R., **2019.** Conventional and new lead-free radiation shielding materials for radiation protection in nuclear medicine: A review. *Radiation Physics and Chemistry*, *165*, p.108439.

[17] Naikwadi, A.T., Sharma, B.K., Bhatt, K.D. and Mahanwar, P.A., **2022.** Gamma radiation processed polymeric materials for high performance applications: a review. *Frontiers in Chemistry*, *10*, p.837111.

[18] Almeshari, M., Sallam, F.H., Tharwat, M., Alzamil, Y., Salih, M., Alshoumr, B., Alyahyawi, A. and El-Taher, A., **2024.** Preparation and structure investigation of polyethylene terephthalate polyester reinforced $Ni_{0.5}Zn_{0.5}Fe_2O_4$ nanoparticles for gamma ray shielding performance. *Physica Scripta*, *99*(5), p.055311.

[19] Sani, A., Zaid, M.H.M., Matori, K.A., Karim, M.K.A. and Wei, L.Z., **2025.** Structural and optical features of new Gd_2O_3-doped zinc boro-tellurite glass systems and computation of radiation shielding attenuation parameters. *Applied Radiation and Isotopes*, *225*, p.112019.

[20] Rani, N., Vermani, Y.K. and Singh, T., **2020.** Gamma radiation shielding properties of some Bi-Sn-Zn alloys. *Journal of Radiological Protection*, *40*(1), pp.296-310.

[21] Prabhu, S., Bubbly, S.G. and Gudennavar, S.B., **2023.** X-ray and γ-ray shielding efficiency of polymer composites: choice of fillers, effect of loading and filler size, photon energy and multifunctionality. *Polymer Reviews*, *63*(1), pp.246-288.

[22] Aliyu, A.S., Aliyu, U.S.A., Hamza, A.M., Nyakuma, B.B., Liman, M.S., Gaya, U.I., Dunama, A.M., Zira, J.D. and Liman, M.M., **2025**. Synthesis and characterisation of rice husk and palm fruit bunch silica: compositional, structural, and thermal analyses. *Biomass Conversion and Biorefinery*, *15*(3), pp.3533-3544.

[23] El-Khayatt, A.M., **2010.** Radiation shielding of concretes containing different lime/silica ratios. *Annals of Nuclear Energy*, *37*(7), pp.991-995.

[24] Mahmoud, K.A., Sayyed, M.I. and Tashlykov, O.L., **2019.** Gamma ray shielding characteristics and exposure buildup factor for some natural rocks using MCNP-5 code. *Nuclear Engineering and Technology*, *51*(7), pp.1835-1841.

[25] Obaid, S.S., Sayyed, M.I., Gaikwad, D.K. and Pawar, P.P., **2018.** Attenuation coefficients and exposure buildup factor of some rocks for gamma ray shielding applications. *Radiation Physics and Chemistry*, *148*, pp.86-94.

[26] Aygün, B., **2019.** Neutron and gamma radiation shielding properties of high-temperature-resistant heavy concretes including chromite and wolframite. *Journal of Radiation Research and Applied Sciences*, *12*(1), pp.352-359.

[27] Alorfi, H.S., Hussein, M.A. and Tijani, S.A., **2020.** The use of rocks in lieu of bricks and concrete as radiation shielding barriers at low gamma and nuclear medicine energies. *Construction and Building Materials*, *251*, p.118908.

[28] Medhat, M., **2012.** Application of gamma-ray transmission method for study the properties of cultivated soil. *Annals of Nuclear Energy*, *40*(1), pp.53-59.

[29] Abdullah, M.A.H., Rashid, R.S.M., Amran, M., Hejazii, F., Azreen, N.M., Fediuk, R., Voo, Y.L., Vatin, N.I. and Idris, M.I., **2022.** Recent trends in advanced radiation shielding concrete for construction of facilities: materials and properties. *Polymers*, *14*(14), p.2830.

[30] Kaky, K.M. and Sayyed, M.I., 2024. The radiation shielding parameters of a standard silica glass system. *Silicon*, *16*(3), pp.1197-1203.

[31] Kaky, K.M. and Sayyed, M.I., **2024.** The radiation shielding parameters of a standard silica glass system. *Silicon*, *16*(3), pp.1197-1203.

[32] Tekin, H.O., Sayyed, M.I. and Issa, S.A., **2018.** Gamma radiation shielding properties of the hematite-serpentine concrete blended with WO_3 and Bi_2O_3 micro and nano particles using MCNPX code. *Radiation Physics and Chemistry*, *150*, pp.95-100.

[33] Allam, E.A., El-Sharkawy, R.M., El-Taher, A., Shaaban, E.R., Massoud, E.E.S. and Mahmoud, M.E., **2022.** Enhancement and optimization of gamma radiation shielding by doped nano HgO into nanoscale bentonite. *Nuclear Engineering and Technology*, *54*(6), pp.2253-2261.

[34] Khalil, A., Bondouk, I.I., Allam, E.A., Nabil, I.M., Al-Abyad, M., Saudi, H., El-Taher, A., Mahmoud, M.E. and Amar, A., **2024.** A binary composite material of nano polyaniline intercalated with Nano-Fe_2O_3 for enhancing gamma-radiation-shielding properties: experimental and simulation study. *Progress in Nuclear Energy*, *169*, p.105067.

© Ariston Publications 2025. All rights reserved.

[35] Rilwan, U., Edeh, S.A., Idris, M.M., Fatima, I.I., Olukotun, S.F., Arinseh, G.Z., Bonat, P.Z., El-Taher, A., Mahmoud, K.A., Hanafy, T.A. and Sayyed, M.I., **2025.** Influence of waste glass on the gamma-ray shielding performance of concrete. *Annals of Nuclear Energy*, *210*, p.110876.

[36] Alafer, F., Sallam, F.H., Al Meshari, M., Alzamil, Y., Abanomy, A., Alhujaili, S. and El-Taher, A., **2024.** The influence of thermal treatment on the structural properties and gamma rays shielding of bentonite clay ceramic. *Radiation Physics and Chemistry*, *217*, p.111531.

[37] Sayyed, M.I., Elbashir, B.O., Tekin, H.O., Altunsoy, E.E. and Gaikwad, D.K., **2018.** Radiation shielding properties of pentaternary borate glasses using MCNPX code. *Journal of Physics and Chemistry of Solids*, *121*, pp.17-21.

[38] El-Sharkawy, R.M., Allam, E.A., El-Taher, A., Shaaban, E.R. and Mahmoud, M.E., **2021.** Synergistic effect of nano-bentonite and nanocadmium oxide doping concentrations on assembly, characterization, and enhanced gamma-rays shielding properties of polypropylene ternary nanocomposites. *International Journal of Energy Research*, *45*(6), pp.8942-8959.

[39] Termote, C., Odongo, N.O., Dreyer, B.S., Guissou, B., Parkouda, C. and Vinceti, B., **2022.** Nutrient composition of Parkia biglobosa pulp, raw and fermented seeds: a systematic review. *Critical Reviews in Food Science and Nutrition*, *62*(1), pp.119-144.

[40] Putra, O.A., Syamputra, D.N.I. and Arafat, F.B., **2025.** Influence of crystal tetrahedral and octahedral voids on the radiation shielding properties of iron-based spinels. *Physics Open*, p.100325.

[41] El-Taher, A., Mahmoud, H.M. and Abbady, A.G., **2007.** Comparative study of attenuation and scattering of gamma-rays through two intermediate rocks. *Indian Journal of Pure and Applied Physics*, *45*(3), pp.198-203.

[42] Nazrin, S.N., Amat, A., Issa, S.A., Zakaly, H.M., Gunasekaran, S.S., Zaman, H.B., Zaid, M.H.M., Tahir, M.H.M., Shaaban, I.A. and Sharma, I., **2024.** Elastic and radiation shielding properties of zinc borotellurite glass systems: The impact of gadolinium oxide. *Optical Materials*, *157*, p.116252.

[43] Alhassan, M., Baraya, J.T. and Garba, A.S., **2023.** Accuracy of Phy-X/PSD software compared to XCOM in the determination of mass attenuation coefficient of glass systems. *Journal of Applied Sciences and Environmental Management*, *27*(5), pp.985-988.

[44] Şakar, E., Özpolat, Ö.F., Alım, B., Sayyed, M.I. and Kurudirek, M., **2020.** Phy-X/PSD: development of a user friendly online software for calculation of parameters relevant to radiation shielding and dosimetry. *Radiation Physics and Chemistry*, *166*, p.108496.

[45] Afaneh, F., Al-Ghamdi, H., Alsaif, N.A., Elsad, R.A., Rammah, Y.S. and Khattari, Z.Y., **2023.** Elastic, mechanical, and radiation shielding behaviors of copper-phosphate binary-glasses with diverse copper valence-states: R (Cu^{+})= Cu^{+}/(Cu^{++} Cu^{++}). *Radiation Physics and Chemistry*, *213*, p.111239.

[46] Rilwan, U., Abdulazeez, M.A., Maina, I., Olasoji, O.W., El-Taher, A., Maisalatee, A.U., Sarki, M.U., Mohammed, G. and Sayyed, M.I., **2025.** Feasibility study on the possibility of utilizing e-nut shell ashes for gamma-radiation protection application. *Radiation Physics and Chemistry*, *233*, p.112748.

 © Ariston Publications 2025. All rights reserved.